High-bandwidth Secondary Voltage and Frequency Control of VSC-based AC Microgrid

Heydari, Rasool; Dragicevic, Tomislav; Blaabjerg, Frede

Published in:
IEEE Transactions on Power Electronics

DOI (link to publication from Publisher):
10.1109/TPEL.2019.2896955

Publication date:
2019

Document Version
Accepted author manuscript, peer reviewed version

This article has been accepted for publication in a future issue of this journal, but has not been fully edited. Content may change prior to final publication. Citation information: DOI 10.1109/TPEL.2019.2896955, IEEE Transactions on Power Electronics

High-bandwidth Secondary Voltage and Frequency Control of VSC-based AC Microgrid

Rasool Heydari, *Student Member, IEEE,* and Tomislav Dragicevic, *Senior Member, IEEE,* and Frede Blaabjerg, *Fellow, IEEE,*

***Abstract*—This paper proposes a novel secondary control strategy for power electronic-based ac microgrid (MG). This approach restores voltage and frequency deviations by utilizing only local variables with very high bandwidth. This is realized with a finite control set model predictive control (FCS-MPC) technique that is adopted in the inner level of primary control of voltage source converters (VSCs). In the outer level of primary control, droop control and virtual impedance loops are exploited to adjust power sharing among different DGs. As inner control level operates with a very high bandwidth, need for filtering of calculated active and reactive powers in the outer level of primary control is insignificant. Therefore, secondary control can be operated with far superior bandwidth compared to the case when conventional cascaded linear control is used. Merits of the proposed approach are investigated analytically with the help of describing function (DF) methodology that allows quasi-linear approximation of the inner control level. Finally, simulation and experimental results are presented.**

***Index Terms*—Distributed secondary control, model predictive control, voltage source converter (VSC), ac microgrid (MG).**

I. Introduction

POWER system integration in a flexible and smart way where supply side and demand side are simultaneously managed has been on technology road-maps for almost every utility and independent system operator (ISO) over the last decade. With the high penetration of clean energy resources, the current power system faces significant challenges. A smart grid (SG) includes distributed energy resources (DER), energy storage systems (ESS) and adjustable loads, which are expected to maximize the flexibility while also decreasing the operation cost of such grids if properly coordinated. A way of simplifying this coordination is the introduction of intelligent microgrids (MGs), which act as intermediate aggregation entities between the individual units and the overall SG [1]. The adoption of MGs for the massive integration of DERs, ESS and loads will reduce the need for complex and centralized management. The increasing penetration of intermittent DERs (e.g., wind and solar) and flexible loads has substantially complicated MGs operation and control. Contrary to the conventional power grid, supply and demand are significantly unpredictable. Furthermore, end-users play a more prominent role in modern power grids [2], [3]. Notably, due to the inherent low inertia characteristic of heterogeneous DERs, frequency and voltage control becomes a challenge in islanded MGs. Small changes in DERs power output may lead to considerable effects on the MG real-time operation and control. Meanwhile, individual loads can have a significant influence on the power balance. Therefore, control strategy plays an essential role in achieving reliable MG operation.

In this context, a hierarchical control structure has been applied to achieve frequency and voltage stability, main grid synchronization, economic energy management, as well as active/reactive power control sharing among DERs, ESS and upstream connected network [4]–[7]. In the hierarchical control strategy, three major control levels are conceived, i.e., primary control (PC), secondary control (SC) and tertiary control (TC) level. Operation time framework and response speed are the main discrepancies among these three control levels [8]. The main aim of the first level (PC) is independent local control of each DER in a MG. It mainly comprises current and voltage control loops, virtual impedance loop and droop control function. In order to compensate for the PC deviations, SC is adopted. The conventional SC technique, based on the central controller, consists of slow frequency and voltage restoration control loops, a central computing unit, and a low bandwidth communication system for sending control signals to each DER [9]–[16].

Since central control decreases the reliability of a MG due to a single point of failure, distributed SC, also referred to as the network control system (NCS), has been suggested [17]–[22].

In [23] a distributed secondary control for voltage deviations via feedback linearization has been presented. However, the approach entirely relies on MG parameters. Distributed finite-time voltage control is stated in [24] and subsequently, MG frequency regulation is addressed while sharing the active power accurately. A general secondary control structure based on the distributed averaging proportional-integral (DAPI) is presented in [25].

Nevertheless, all aforementioned control structures have several deficiencies:

First, low bandwidth SC is employed to compensate for frequency and voltage deviations which make the MG very sluggish. Furthermore, conventional multi-loop linear control structure has inherently slow dynamic performance since the outer loop should be designed with smaller bandwidth compared to the innermost control loop. Practically, the operation of MG at nominal voltage and frequency values is essential for sensitive loads in SG. For instance, based on the IEC62040 standard, voltage amplitude drop to less than 10% should be recovered within first 0.1 seconds in uninterrupted power supply (UPS) applications. Therefore, fast response is a highly desirable feature. Moreover, conventional control structures are heavily dependent on knowing the MG parameters, which limit the robustness. Finally, accurate power sharing is not satisfied in classical approaches during transient periods due to

R. Heydari, T. Dragicevic and F. Blaabjerg are with the Department of Energy Technology, Aalborg University, Aalborg, DK, 9220, Denmark e-mail: (rah@et.aau.dk, tdr@et.aau.dk, fbl@et.aau.dk).

This article has been accepted for publication in a future issue of this journal, but has not been fully edited. Content may change prior to final publication. Citation information: DOI 10.1109/TPEL.2019.2896955, IEEE Transactions on Power Electronics

the slow response. Therefore, a super-high bandwidth PC has been introduced in [26]. We then built upon this approach to propose super-high bandwidth centralized SC [27]. However, tunning of high bandwidth SC parameters and MG stability analysis are not acknowledged in that paper. The fully distributed manner with higher bandwidth and a comprehensive comparison are also presented here.

The major novelties of our approach are:

1) Compared to conventional control strategies, the suggested scheme compensates the steady state frequency/voltage deviation much faster than conventional methods using a fully distributed approach.

2) The load frequency analysis of the proposed method shows that the approach is stable with higher bandwidths compared to the literature. Describing function (DF) approach is applied to prove the bandwidth improvement analytically. Furthermore, experimental results verify the efficiency of the proposed algorithm.

3) Contrary to the classical approaches, active and reactive power sharing are maintained during both steady-state and transients.

The rest of the paper is organized as follows. Section II gives a brief introduction on the MG dynamic model and hierarchical control strategy, especially PC and SC approaches. Details of the proposed distributed FCS-MPC based SC algorithm are given in Section III. Furthermore, the DF method is illustrated to prove the stability and bandwidth improvements. Simulation and experimental results of the proposed approach are presented in Section IV and Section V respectively. Finally, Section VI concludes the paper with a brief summary.

II. Conventional ac MG Control

MG is conceptually considered to operate in connection to the main grid, albeit by the bypass switch (see Fig. 1) it should be able to transfer power from grid connected to stand alone operation, which is the major focus of this paper. As it can be seen from the Fig. 1, ac MG comprises several VSC-based DGs, which exchange the electrical power with the common ac bus. Furthermore, they also regulate the output voltage of VSCs and frequency of the MG. Thus, VSCs are the backbone of the power electronic based MG. They can be classified into the three main categories, i.e., grid feeding, grid forming and grid supporting VSCs. The latter ones are crucial elements in operation of paralleled VSCs [28]. The proposed distributed control structure of MG is made of two local layers: PC of voltage and current, which corresponds to the grid-supporting VSC, and SC, which achieves frequency and voltage regulation in an islanded MG [29]. TC, which optimizes the MG operation in the highest level is out of the scope of this paper.

A. Local voltage and current control

Firstly, the PC is utilized in order to regulate the voltage and frequency locally during stand-alone operation. Second important role of PC is power sharing (active and reactive) among DGs and providing the plug-and-play capability for them [30]–[32]. The infrastructure of major control loops

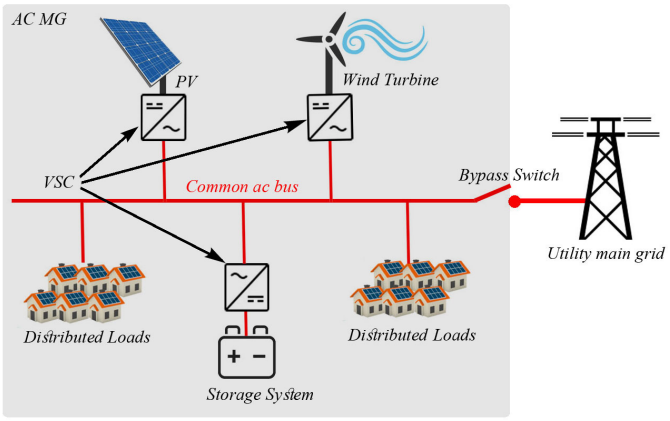

Fig. 1. Diagram of a voltage source converter based microgrid having different sources and loads.

is settled in the PC, i.e., the independent inner current and voltage loops, which are referred to as zero-level control [33], and the outer droop and virtual impedance loop.

The nested voltage and current control loops should be design with higher bandwidth compared to the outer loops. Voltage control loop regulates the capacitor voltage and provides the reference to the inner current control loop. Proportional integral derivative (PID), and proportional resonant controllers are typically used for inner control loops [34], [35]. Therefore, the dynamics of the inner loops need to be much faster than outer ones if linear control is used [36].

B. Virtual Impedance and Droop

The conventional power control of PC is implemented by a droop control strategy for active and reactive power sharing. The dominant idea of droop controller is to emulate the behaviour of a synchronous machine, which decreases the frequency while the active power is increased. This feature can be achieved in the paralleled operation of VSCs by applying the $P-\omega$ and $Q-V$ droop characteristics. The VSC can be modeled as an ac power generation source with the voltage amplitude of E and power angle of δ. Considering common ac MG bus voltage is $V_{MG}\angle 0$ and the connection line impedance is $Z\angle\theta$, the complex exchange power can be achieved as follows:

$$S = V_{MG}I^* = \frac{V_{MG}E\angle\theta-\delta}{Z} - \frac{V_{MG}^2\angle\theta}{Z}, \tag{1}$$

therefore, active and reactive power can be calculated as follows:

$$\begin{cases} P = \frac{V_{MG}E}{Z}\cos(\theta-\delta) - \frac{V_{MG}^2}{Z}\cos(\theta) \\ Q = \frac{V_{MG}E}{Z}sin(\theta-\delta) - \frac{V_{MG}^2}{Z}sin(\theta) \end{cases}. \tag{2}$$

Since active and reactive power exchange rely on both voltage and power angle, a virtual impedance is employed. Virtual impedance concept enforces the output impedance, seen by VSC, to be purely inductive or purely resistive. Thus, the power angle is assumed to be $\theta = 0$ and $\theta = 90$ for the inductive and resistive virtual impedance respectively. Since

This article has been accepted for publication in a future issue of this journal, but has not been fully edited. Content may change prior to final publication. Citation information: DOI 10.1109/TPEL.2019.2896955, IEEE Transactions on Power Electronics

resistive impedance value does not rely on the frequency and non-linear load effects, it would be better to implement resistive virtual impedance [37]. If the phase angle difference between the voltage of VSC and ac common bus is small enough, then, $cos\delta \approx 1$ and $sin\delta \approx \delta$. Accordingly, the droop characteristic can be achieved as follows:

$$\begin{cases} \omega_{ref} = \omega_{nom} + D_Q Q \\ V_{ref} = V_{nom} - D_P P \end{cases}, \tag{3}$$

where, ω_{ref} stands for reference frequency and V_{ref} refers to reference voltage amplitude, whereas, k_Q and k_P are droop coefficients.

Droop coefficients (D_P and D_Q) can be selected based on the power rating of VSCs and maximum admissible deviation of voltage and frequency. Droop coefficients can be determined by (4), for a MG with N converters and resistive output impedance [38], [39]:

$$\begin{cases} D_{p_1} P_1 = D_{p_2} P_2 = \cdots = D_{p_N} P_N = \Delta v_{max} \\ D_{Q_1} Q_1 = D_{Q_2} Q_2 = \cdots = D_{Q_N} Q_N = \Delta \omega_{max} \end{cases}, \tag{4}$$

where P_N and Q_N refer to nominal active and reactive power output of nth VSC respectively, while $\Delta\omega_{max}$ and Δv_{max} are maximum admissible deviations of frequency and voltage, respectively.

Although cascaded control technique is widely used, this structure performs as a low-pass filter with lower bandwidth in contrast with the inner cascaded linear loops. Thus, the overall response time is very slow. Most notably, inner control loops in PC have a finite bandwidth. Therefore, the bandwidth of low-pass filters in the power calculation loops needs to be intentionally set a further order of magnitude lower to avoid undesirable interactions. For this reason, the overall system behaves extremely slow. Furthermore, the performance of power converter when operating away from the equilibrium is not the same, hence, the robustness is limited.

C. Secondary Control of VSC-based MG

The SC is required to compensate for voltage amplitude and frequency deviations caused by PC. Conventional SC is based on the MG Central Control (MGCC) and low bandwidth communication network [40]. In this structure, the MG frequency and each DG voltage amplitude are compared with the references concerning compensations.

1) Frequency control: Frequency restoration in SC is implemented by sending a complementary signal to droop in order to regulate the reference frequency. The compensatory signal can be acquired by:

$$\delta\omega = k_{p_\omega}(\omega^\star_{ref} - \omega_{MG}) + k_{i_\omega}\int(\omega^\star_{ref} - \omega_{MG})dt + \Delta\omega_s, \tag{5}$$

while k_{P_ω} and k_{I_ω} are the controller parameters of PI. The supplementary term, $\Delta\omega_s$ in (5) refers to the synchronization term of grid-connected MG. Whereas in grid-connected operation, the main grid determines the corresponding reference values, $\Delta\omega_s$ will be zero in island-alone MG. The frequency of MG (ω_{MG}) compared to the corresponding reference ($\omega^\star_{ref}$) and compensator signal $\delta\omega$ is sent to the available DGs to adjust the MG frequency. The main inconvenience of such structure is that a failure of MGCC will lead to SC collapse.

In distributed manner, the SC level is settled in each DG as a local controller while communication link at the upper control level transfers measured data of each unit. SC collects all data from other DG units, averages them and broadcasts its value to the other DGs. The MG set-point frequency is compared with the average measured data and the proper signal is sent to the inner PC level, then removing the steady-state errors. The frequency compensation signal can be achieved from (6):

$$\delta\omega_{DG_k} = k_{p_\omega}(\omega^\star_{ref} - \overline{\omega}_{DG_k}) + k_{i_\omega}\int(\omega^\star_{ref} - \overline{\omega}_{DG_k})dt, \tag{6}$$

$$\overline{\omega}_{DG_k} = \frac{\sum_{i=1}^{N}\omega_{DG_i}}{N}, \tag{7}$$

while $\overline{\omega}_{DG_k}$ and $\omega^\star_{ref}$ are the averages of frequency for all DGs and reference frequency of the MG, respectively. Obviously, $\delta_{\omega_{DG_k}}$ is a fitting signal sent from local SC to PC in every sampling time and N is the number of DGs.

2) Voltage control: conventionally, when the MG bus voltage deviates from the reference rms value, a smooth PI controller regulates the bus voltage with a compensation signal being sent to each DG via low bandwidth communication. Similar to frequency control (equation (5)), the voltage restoration signal can be given as:

$$\delta V = k_{p_v}(V^\star_{ref} - V_{MG}) + k_{i_v}\int(V^\star_{ref} - V_{MG})dt, \tag{8}$$

where k_{P_v} and k_{I_v} refer to PI controller constants of the voltage SC. The voltage compensator signal (δV) is sent to each DG to regulate droop control error.

In a distributed structure, each local SC calculates the average of exchanged voltage amplitude via communication broadcast and compares it with the reference value of the voltage. Then, an appropriate signal, i.e., $\delta_{V_{DG_k}}$ changes the set point of PC to compensate for the MG voltage deviations.

$$\delta V_{DG_k} = k_{p_v}(V^\star_{ref} - \overline{V}_{DG_k}) + k_{i_v}\int(V^\star_{ref} - \overline{V}_{DG_k})dt, \tag{9}$$

$$\overline{V}_{DG_k} = \frac{\sum_{i=1}^{N}V_{DG_i}}{N}, \tag{10}$$

where $\overline{V}_{DG_k}$ refers to the average of voltages broadcasted from each DG in every sampling time. The proposed SC signals are implemented to primary droop control to adjust the reference voltage and frequency. It is worth to note that the SC parameters should be selected so that its response time is approximately an order of magnitude slower than PC level. Therefore, by increasing the PC bandwidth, the SC bandwidth can inherently be increased as well. This approach, which

This article has been accepted for publication in a future issue of this journal, but has not been fully edited. Content may change prior to final publication. Citation information: DOI 10.1109/TPEL.2019.2896955, IEEE Transactions on Power Electronics

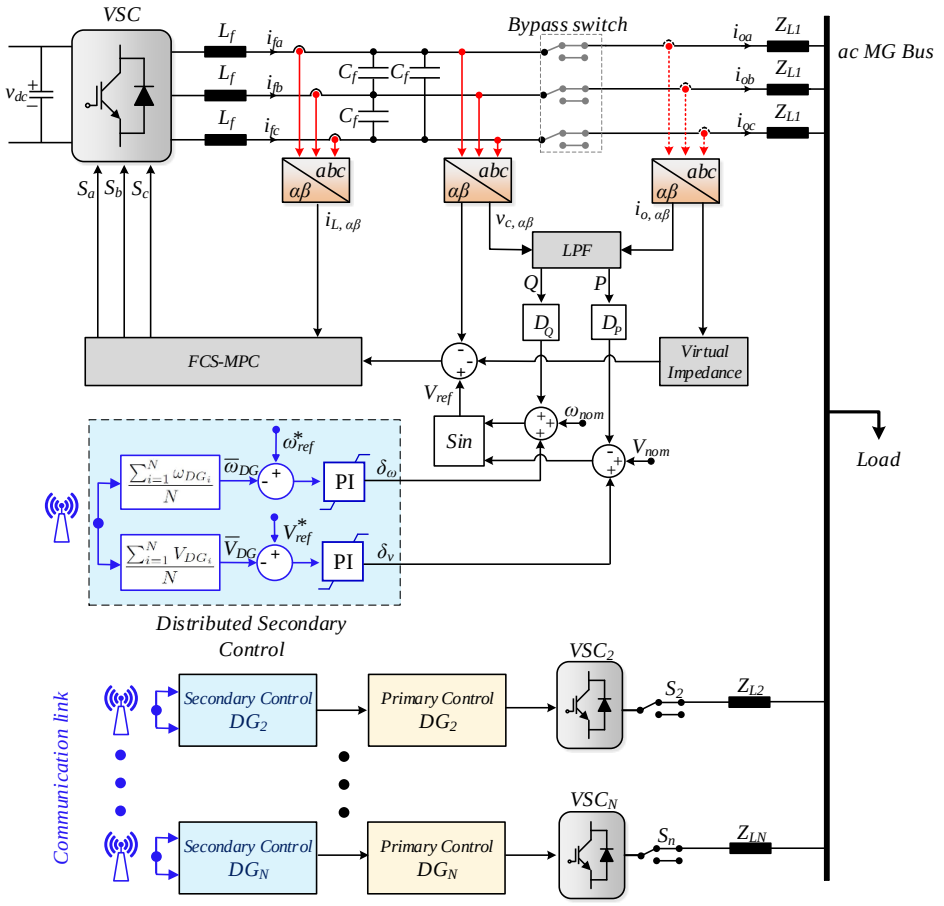

Fig. 2. Proposed scheme of primary and distributed secondary control of the VSC-based microgrid.

forms the essential contribution of the paper, is discussed in the following section.

III. Proposed Control Based on the Robust FCS-MPC

Motivated by the slow dynamic response of the distributed SC approaches of the state of the art, a new control structure based on the FCS-MPC is proposed here as an alternative solution for the fast MG frequency and voltage regulations.

A. FCS-MPC operating principle

In the FCS-MPC approach, an appropriate control signal is calculated based on the prediction from a system model and a cost function (CF). The main control elements of the power electronic based MG are VSCs, which will be modeled in this section. The eight switching states of two-level three-phase VSC are shown in Fig. 3. The three main gating signals S_a, S_b and S_c constitute the VSC output. By adapting the complex Clarke transformation, eight (2^3) feasible switch configuration are obtained in $\alpha - \beta$ frame, as demonstrated in Fig. 3.

In order to suppress the switching harmonics, the VSC is connected to the load through a three-phase LC filter (see Fig. 2). The output current and the filter current (L_f) are presented by L_o and i_f, respectively. Thus, the following current and voltage vectors are defined:

$$i_o = [i_{ou} \quad i_{ov} \quad i_{ow}]^T, \tag{11}$$

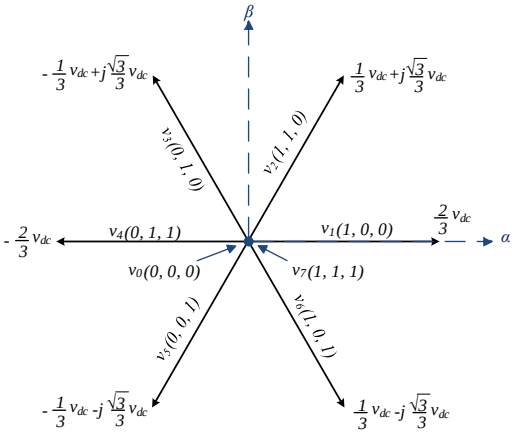

Fig. 3. Voltage vectors and switching states generated by a two-level three-phase VSC.

$$i_f = [i_{fu} \quad i_{fv} \quad i_{fw}]^T, \tag{12}$$

$$v_f = [v_{fu} \quad v_{fv} \quad v_{fw}]^T, \tag{13}$$

capacitor voltage v_f across the C_f and inductor current i_f are the state variables of the system. The system model is based on the $\alpha\beta$ reference frame. Accordingly, all generic three phase variable vectors $z_{uvw} \in \mathbb{R}^3$ are transferred to

This article has been accepted for publication in a future issue of this journal, but has not been fully edited. Content may change prior to final publication. Citation information: DOI 10.1109/TPEL.2019.2896955, IEEE Transactions on Power Electronics

the two-dimensional vector $z_{\alpha\beta} \in \mathbb{R}^2$ by employing Clarke transformation T as follows:

$$\overline{z_\alpha} + j\overline{z_\beta} = T[z_u \quad z_v \quad z_w]', \tag{14}$$

where

$$T = \frac{1}{3}\left[1 \quad e^{j\frac{2}{3}\pi} \quad e^{j\frac{4}{3}\pi}\right]. \tag{15}$$

consequently, based on the Kirchhoff's law, the converter output voltage and current can be indicated in the state-space form, where $\bar{i}_f$ and $\overline{v}_f$ are the state vector in $\alpha\beta$ stationary reference frame, *A* is the system matrix and *B* is the control matrix as follows:

$$\frac{d}{dt}\begin{bmatrix} \bar{i}_f \\ \overline{v}_f \end{bmatrix} = A\begin{bmatrix} \bar{i}_f \\ \overline{v}_f \end{bmatrix} + B\begin{bmatrix} \overline{v}_i \\ \bar{i}_0 \end{bmatrix}, \tag{16}$$

$$A = \begin{bmatrix} -\frac{R_f}{L_f} & -\frac{1}{L_f} \\ \frac{1}{C_f} & 0 \end{bmatrix}, \tag{17}$$

$$B = \begin{bmatrix} \frac{1}{L_f} & 0 \\ 0 & -\frac{1}{C_f} \end{bmatrix}, \tag{18}$$

where R_f, L_f and C_f are resistance, inductance and capacitance of each leg of the filter, respectively. The state variables of $\bar{i}_f$ and $\overline{v}_f$ are inductor current and capacitor voltage respectively.

The major objective of the control strategy is to appropriately adapt the input voltage $\overline{v}_i$ so that the output voltage $\overline{v}_f$ can follow the reference voltage trajectory accurately.

The fundamental operation of MPC is based on the prediction value of $\overline{v}_f$ and $\bar{i}_f$ and applying optimal $\overline{v}_i$ according to the cost function. The corresponded vector with minimum CF value is enforced to the converter. Thus, the main part of the MPC approach is determining CF appropriately. In order to minimize the voltage deviation and switching loss with consideration the current constraint the following general CF is used.

$$CF: \sum_{i=k}^{k+N-1} \left(\|\overline{v}_e(i)\|^2 + \xi_{lim}(i) + \zeta_w SW^2(i)\right), \tag{19}$$

where $\overline{v}_e(i)$ is the prediction error, $\xi_{lim}(i)$ exposes the current constraint, which is shown in (21) and switching effort (SW) with a weighting factor (ζ_w) can be expressed as given in (22). An artificial neural network (ANN) approach is presented in [41] and employed in this paper for the selection of weighting factors in the CF.

$$\overline{v}_e(i) = \overline{v}_f^*(i) - \overline{v}_e(i), \tag{20}$$

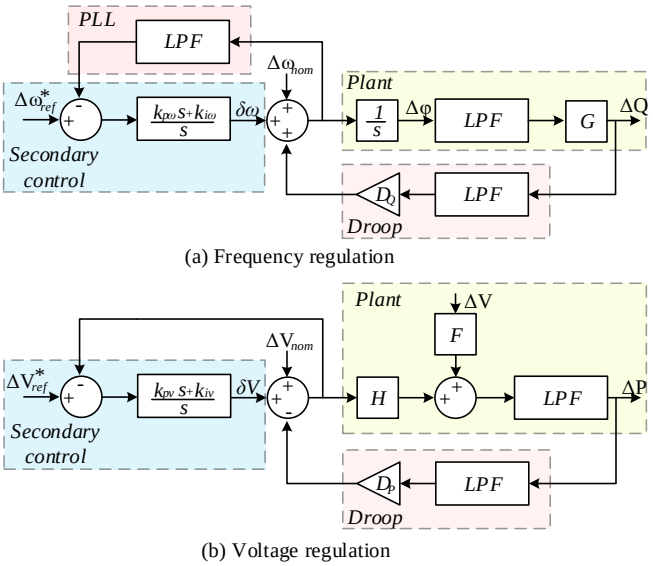

Fig. 4. Small-signal representation of frequency and voltage control. (a) Frequency regulation. (b) Voltage regulation.

$$\xi_{lim}(i) = \begin{cases} 0, & \text{if } |i_f(i)| \leq i_{max} \\ \infty, & \text{if } |i_f(i)| > i_{max} \end{cases}, \tag{21}$$

$$SW(i) = \sum |u(i) - u(i-1)|. \tag{22}$$

In order to decrease the total harmonic distortion (THD), a regulator should follow the voltage references and its derivative simultaneously [26]. Therefore, another term is added to the CF to minimize the voltage derivative error as follows:

$$\left(\frac{d\overline{v}_f^*(t)}{dt} - \frac{d\overline{v}_f(t)}{dt}\right) = (C_f\omega_{ref}v_{f\beta}^* - i_{f\alpha} + i_{o\alpha})^2 + (C_f\omega_{ref}v_{f\alpha}^* + i_{f\beta} - i_{o\beta})^2, \tag{23}$$

where ω_{ref} and v_{ref} are frequency and voltage of the reference signal respectively. Thus the total CF for $N = 1$ can be written as follows:

$$\begin{aligned} CF: &(v_{f\alpha}^* - v_{f\alpha})^2 - (v_{f\beta}^* - v_{f\beta})^2 \\ &+\mu\left((C_f\omega_{ref}v_{f\beta}^* - i_{f\alpha} + i_{o\alpha})^2 + (C_f\omega_{ref}v_{f\alpha}^* + i_{f\beta} - i_{o\beta})^2\right) \\ &+\xi_{lim}(i) + \zeta_w SW^2(i). \end{aligned} \tag{24}$$

As it can be seen from the Fig. 3, every VSC receives the reference voltage from the upper loops which are droop and resistive virtual impedance loops. Consequently, the PC level is completed [**?**], [27]. SC at upper level regulates the reference set point. The proposed strategy with presented FCS-MPC strategy in PC are utilized into the MG with distributed structure. The simulation results will be demonstrated in the following section.

This article has been accepted for publication in a future issue of this journal, but has not been fully edited. Content may change prior to final publication. Citation information: DOI 10.1109/TPEL.2019.2896955, IEEE Transactions on Power Electronics

B. Distributed SC modeling and parameters adjustment

In order to adjust the parameters of SC, and analyze the MG stability, a dynamic model of distributed SC and frequency response analysis have been performed. Block diagrams are indicating dynamic model of the voltage and frequency control in the s-domain as shown in Fig. 4. The model includes droop control, plant and distributed SC structure. Furthermore, a phase locked loop (PLL) is employed to extract the frequency of the system in the frequency control model [42]. As it can be seen, a low-pass filter (LPF) is utilized in the droop function and another LPF is employed for the plant model in order to calculate active and reactive power from the instantaneous power. It is worth to note that the bandwidth of LPF should be smaller than the inner loops. As mentioned in previous section, the compensating signals obtained from SC through (6) and (9) are added to the droop function in order to shift the droop characteristics and regulate the voltage and frequency. As shown in [26] , FCS-MPC based PC operates with significantly higher bandwidth compared to the case when cascaded linear control is used. In this section, the band-width improvement is also analytically quantified.

Based on the Mason's theorem and Fig. 4, the frequency and voltage reference can be derived as:

$$\Delta\omega_{ref}(s) = \Delta\omega_{nom}(s) + [\Delta\omega^{\star}_{ref}(s) - \Delta\omega_{ref}(s) \times (\tfrac{1}{\tau s+1})] \times [k_{p\omega} + \tfrac{k_{i\omega}}{s}] + \tfrac{D_Q}{\tau_d s+1} \times \Delta Q(s), \tag{25}$$

$$\Delta V_{ref}(s) = \Delta V_{nom}(s) + [\Delta V^{\star}_{ref}(s) - \Delta V_{ref}(s)] \times [k_{pv} + \tfrac{k_{iv}}{s}] - \tfrac{D_p}{\tau_d s+1} \times \Delta P(s). \tag{26}$$

The transfer function can be derived to create open loop forward path expressions for the dynamic model of the regulator in Fig. 4. Hence, frequency response and system stability analysis can be applied. For the frequency regulator (Fig. 4(a)), and voltage regulation control loop (Fig. 4(b)) the forward path transfer functions can be achieved as:

$$\frac{\Delta Q(s)}{\Delta\omega(s)} = \frac{\frac{k_{p\omega}s+k_{i\omega}}{s} \times \frac{1}{s} \times \frac{1}{\tau_p s+1} \times G}{1 + \frac{1}{s} \times \frac{1}{\tau_p s+1} \times G \times \frac{D_Q}{\tau_d s+1}}, \tag{27}$$

$$\frac{\Delta P(s)}{\Delta V(s)} = \frac{\frac{k_{pv}s+k_{iv}}{s} \times H \times \frac{1}{\tau_p s+1}}{1 - \frac{1}{\tau_p s+1} \times \frac{D_p}{\tau_d s+1}}, \tag{28}$$

where, blocks of G and H in the proposed dynamic model can be obtained based on the (2) as follows:

$$G = -\frac{V_{MG}E_i \cos\phi_i}{R_i}, \tag{29}$$

$$H = \frac{2V_{MG} - E_i \cos\phi_i}{R_i}, \tag{30}$$

The LPF at the plant block in Fig. 4 determines the bandwidth of primary control and inner loops. For the conventional control structure, voltage regulator at PC can be assumed to be around 150 Hz (this has been designed in [43] for the parameters similar to the system used in this paper). Thus, by applying a LPF with a cutoff frequency of 150 Hz the dynamic model of conventional control structure is accomplished.

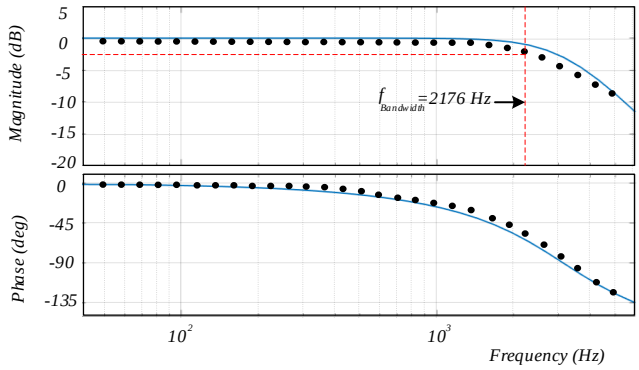

Fig. 5. Frequency response of the voltage reference tracking performance (black dots) and estimated low-pass Butterworth filter (blue line).

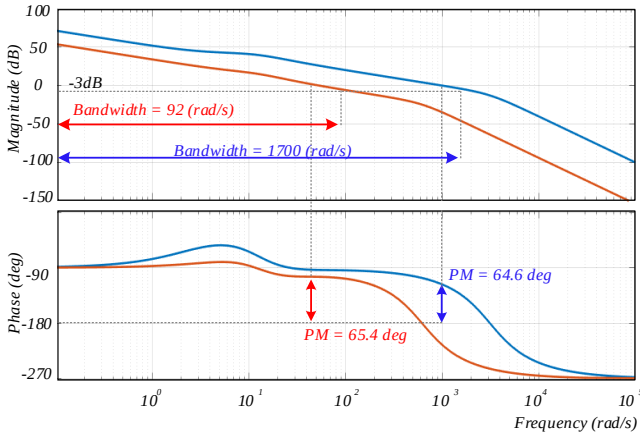

Fig. 6. Bode diagram for the conventional control structure (red line) and proposed FCS-MPC based control approach (blue line).

C. Describing Function analysis

The DF analysis is a possible technique for the analysis of nonlinear systems. In order to achieve the frequency model of FCS-MPC based plant and its LPF characteristic, a frequency analysis DF method presented in [44] is employed. The basic idea is to replace nonlinear element with a DF which can be expressed by the ratio of the output first harmonic component and the applied input sinusoidal signal. Based on the DF method, a nonlinear element can be represented by the equivalent linear frequency response if a perturbation signal enforced to the nonlinear part excites a sinusoidal signal at the same frequency. Considering a sinusoidal input signal, the nonlinear output can be expressed based on the Fourier transform as follows:

This article has been accepted for publication in a future issue of this journal, but has not been fully edited. Content may change prior to final publication. Citation information: DOI 10.1109/TPEL.2019.2896955, IEEE Transactions on Power Electronics

$$y(t) = A_0 + \sum_{n=1}^{\infty} (A_0 \cos n\omega t + B_n \sin n\omega t) \\ = A_0 + \sum_{n=1}^{\infty} Y_n \sin(n\omega t + \varphi_n) \quad (31)$$

Suppose $n > 1$ and $A_0 = 0$, the output signals Y_n are neglectable. Thus, the nonlinear element output can be represent by the plural ratio of the sinusoidal input and the first harmonic of nonlinear link. Consequently, prevailing frequency domain methods can be applied for stability analysis in a nonlinear system which is represented by DF [45].

To this purpose, a small signal perturbation frequency sweep, varied from 50 Hz to 5 kHz in 29 logarithmically spaced discrete steps, is performed. In this case, the voltage amplitude is kept constant while the frequency is varied, and 29 simulations are accomplished. Fig. 5 demonstrates the measured amplitude and phase of the load voltage for each frequency step. Then a low-pass Butterworth filter with a cutoff frequency of 500 Hz is implemented to approximate the frequency performance of FCS-MPC based plant. According to Fig. 5, it is convenient to approximate the plant with a Butterworth filter. Therefore, the dynamic model of the proposed MG control structure is accomplished by applying Butterworth filter with a cutoff frequency of 500 Hz in the plant block (see Fig. 4).

Finally, in order to adjust the SC level, the PI parameters (k_p and k_i) should be selected so that firstly, the phase margin and gain margin are in the acceptable range and, thereby, the MG is maintained stable. Then, fast set-point tracking and good dynamic response are achieved.

The Bode plot of Fig. 6 shows frequency responses of the proposed distributed SC and conventional control structure. As it can be seen, by utilizing the FCS-MPC, the SC can be operated in higher bandwidth compared to the conventional strategies. Consequently, the overall dynamic performance of the MG is much higher.

IV. Simulation Results

A simplified 200 V, 50 Hz islanded MG with two VSCs and LC filters, shown in Fig. 2, is simulated using the parameters given in Table I. Three different test cases have been scrutinized to perform the simulation results. In order to evaluate the effectiveness of the proposed control structure, MG power sharing with equal and unequal power rate for two VSCs is considered. Furthermore, voltage and frequency restorations have been verified. It is worth to note that in order to have a decisive comparison, the simulated model parameters were selected to be similar with the literature (e.g., [21]).

A. Case 1: Equal power sharing

The simulation setup consists of two full bridge 3-phase VSCs with LC filters which feed the ac bus. In this part, the proposed method is verified by changing the load and configuration as follow:

1) $t = 0.0$ s, primary and secondary control is activated.
2) $t = 0.06$ s, one load is connected.

Fig. 7 represents the transient active and reactive power sharing of the MG during the load change. The proposed distributed SC is able to share active and reactive power between DGs sufficiently, while the load changes at $t = 60$ ms. Furthermore, compared with the conventional control technique that needs low-pass filters with a bandwidth approximately an order of magnitude lower than underlying loops, in proposed strategy filtering with high bandwidth leads to an instant response to power load change. The reason for this very fast response is that by using FCS-MPC technique in PC, the bandwidth of voltage control up to the physically realizable limit, which is defined by the system parameters. Moreover, the fluctuations in the measured active and reactive power (P and Q) caused by harmonics get almost nullified by SC coefficients. Thus, the interaction between the outer and inner loops is no longer an issue.

B. Case 2: Unequal power sharing

Since the islanded MG comprise the DGs with distinct power rates, another experiment with different power rate of DGs is shown in Fig. 8. In this case, power rating for the VSC_2 is twofold of the VSC_1, hence, active and reactive power sharing should be based on the different amount of power ratings. As it can be demonstrated, the proposed control structure sufficiently shares corresponding active and reactive power between two DGs with various power rates and fast dynamic performance.

C. Case 3: Voltage and frequency restoration

As it can be seen from Fig. 9, the proposed distributed control scheme restores frequency and voltage deviations immediately. Based on the IEEE 1574 standard, allowable frequency deviations is 1% for under frequency and 0.8% for over frequency in MGs and the allowable restoration time is 160 ms. Obviously, the control strategy respects the standards by a vast margin and several order of magnitude faster than linear control techniques introduced in the literature (e.g. see Fig. 10 from [42]).

D. Case 4: Comprehensive comparison

To evaluate the performance of the proposed control structure, the linear multiple control loop structure which is widely used in the parallel operation of VSCs and presented in [43] is also implemented to serve as a benchmark. Generally, in the linear control structure, the inner current control loop is used to track the command signal from the outer voltage loop. The inner current and voltage loops are designed based on the serial tuning, hence, innermost control loop the first to be tuned pursuant to eligible bandwidth. Therefore, the outer loop is designed with approximately two orders of magnitude lower bandwidth compared to the inner loop which leads to slow dynamic response. This nested control loop structure and pulse-width-modulated (PWM) delays make the whole MG sluggish. Conventional multi-loop control structures compensate for voltage and frequency deviations in order of multi seconds. In order to increase the bandwidth of cascaded control loops, dynamic decoupling between the inductor current and capacitor

This article has been accepted for publication in a future issue of this journal, but has not been fully edited. Content may change prior to final publication. Citation information: DOI 10.1109/TPEL.2019.2896955, IEEE Transactions on Power Electronics

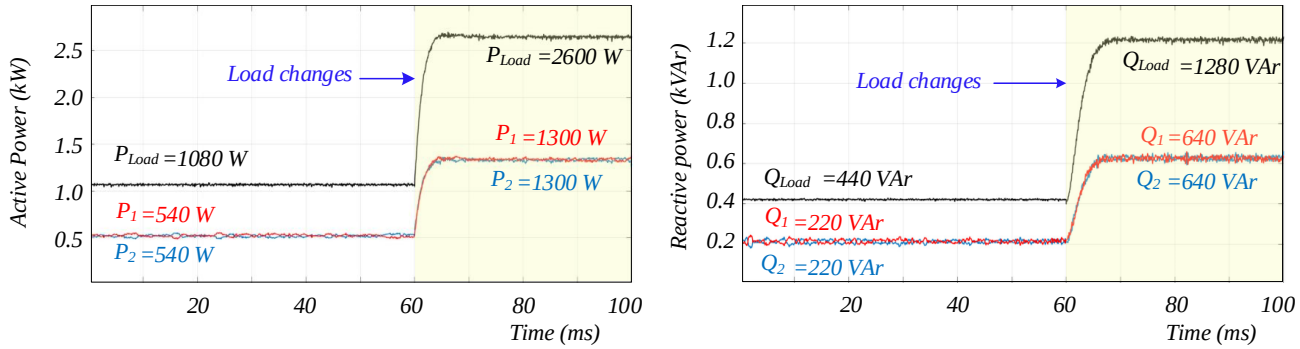

(a) Active power sharing (b) Reactive power sharing

Fig. 7. Transient power sharing accuracy between two VSCs with equal power rating during a load change. (a) Active power sharing. (b) Reactive power sharing.

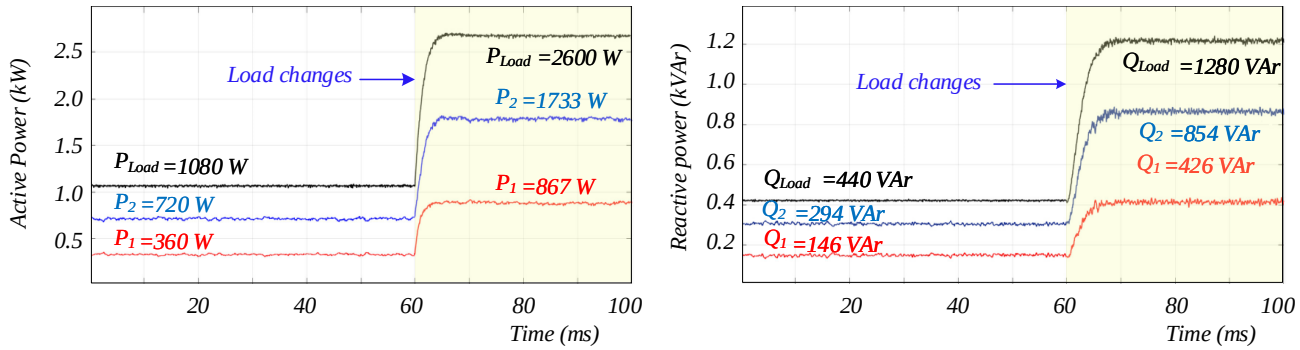

(a) Active power sharing (b) Reactive power sharing

Fig. 8. Power sharing accuracy of two VSCs with different power ratings during a load change. (a) Active power sharing. (b) Reactive power sharing.

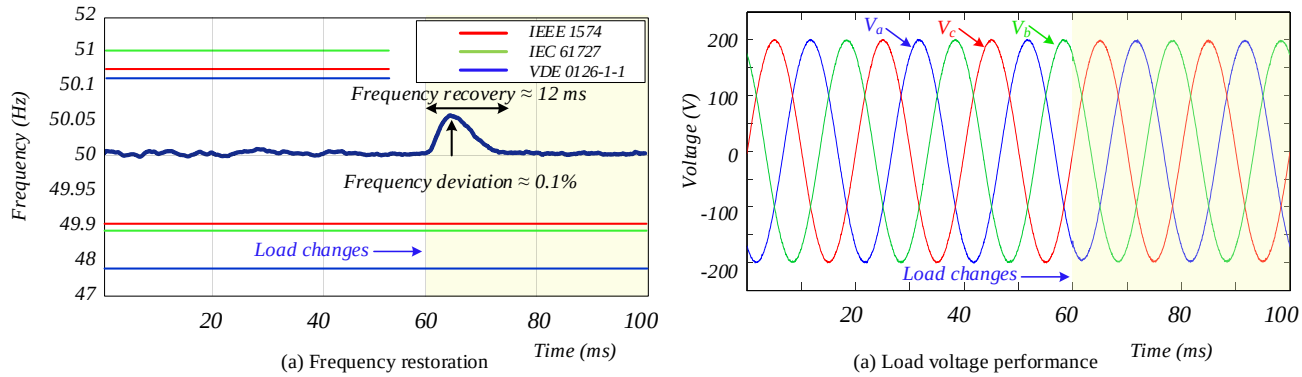

(a) Frequency restoration (a) Load voltage performance

Fig. 9. Validation of the proposed approach during a load change. (a) Frequency restoration and marginal standards. (b) Phase voltages at the point of common coupling.

voltage is presented in [43]. However this approach is not fast enough compared to the proposed approach. Fig. 10 demonstrates frequency and voltage restoration employing cascaded linear control structure presented in [43] in comparison with the proposed FCS-MPC based control scheme. As it can be seen, the dynamic response of the proposed structure is faster than linear multi-loop controllers. Fig. 10 (a) shows frequency restoration employing linear multiple control loops (red line) in comparison with the proposed FCS-MPC approach (blue line). It can be seen that the proposed controller compensates for the frequency deviations far superior to the linear control structure. Fig. 10 (b) shows voltage restoration applying linear controller. Compared to the Fig. 9 (b) which shows voltage regulation performance of the proposed approach, dynamic response of linear controller is very slow.

E. Case 5: Communication link deficiencies

The hierarchical control structure relies on the shared data and communication link among DGs. Therefore, data dropout and communication delay degrade the accomplishment of control structures. In this section, the effect of communication delay on the proposed control structure is illustrated. Fig. 11 shows the frequency restoration with 10 ms delay on

This article has been accepted for publication in a future issue of this journal, but has not been fully edited. Content may change prior to final publication. Citation information: DOI 10.1109/TPEL.2019.2896955, IEEE Transactions on Power Electronics

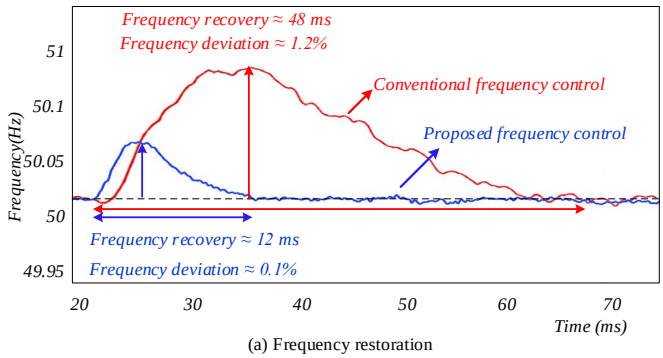

(a) Frequency restoration

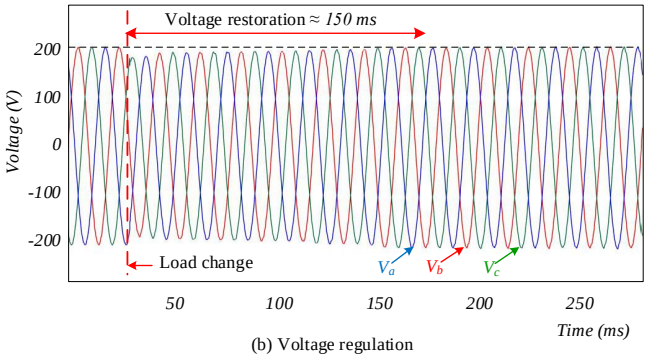

(b) Voltage regulation

Fig. 10. Performance of proposed control structure in comparison to the conventional cascaded linear control methods. (a) Frequency restoration (blue: proposed control approach, red: linear cascaded control); (b) Voltage regulation by employing linear control structure

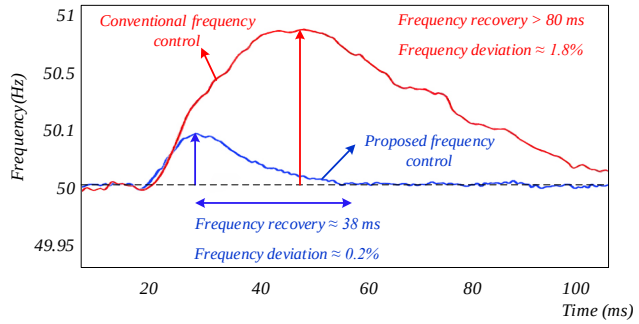

Fig. 11. Frequency restoration with 10 ms delay on the communication link (blue: proposed control approach, red: linear cascaded control.)

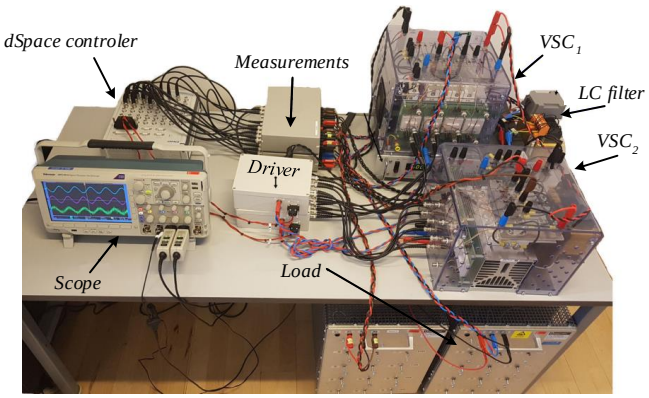

Fig. 12. Experimental setup.

communication link among DGs (red line shows the conventional linear control, and the blue line shows the proposed frequency control structure). Accordingly, SC receives the shared required data (frequency and voltage) with 10 ms delay on communication network link. Conventional linear control structure with 10 ms data transmission delay cannot regulate the MG frequency during 80 ms. However, the proposed control structure compensates for frequency deviations in 38 ms. As it can be seen, the proposed control approach regulates the MG frequency faster than the conventional multi-loop

TABLE I. TEST SYSTEM PARAMETERS USED IN SIMULATIONS AND EXPERIMENTS.

Parameter	Symbol	Value
DC Voltage	V_{dc}	$520\ V$
Nominal voltage amplitude	V_{nom}	$200\ V$
Nominal frequency	f_{nom}	$50\ Hz$
LC filter	$L_f,\ C_f$	$L_f = 2.4\ mH, C_f = 15\ \mu F$
Sampling time	T_s	$25\ \mu s$
Droop coefficients	$D_p,\ D_q$	$D_p = 0.005\ V/W$ $D_q = 0.002\ rad/sVar$
Line impedance	$R_l,\ L_l$	$R_l = 0.1\ \Omega,\ L_l = 2.4\ mH$
Virtual resistance	R_v	$2\ \Omega$
PI parameters	$k_p,\ k_i$	$k_p = 1,\ k_i = 3\ s^{-1}$

structure even with communication delay. It is worth to note that compared to the Fig. 10 (a) that shows the frequency regulation with ideal communication link, the proposed control structure, with 10 ms delay (blue line in Fig. 11), compensates for frequency deviation faster than conventional linear methods with ideal communication link (red line in 10 (a)).

V. EXPERIMENTAL RESULTS

The performance of the approach is evaluated practically by applying two 18 kW-VSCs connected to LC filters. A DC power supply (Delta Elektronika SM600-10) is utilized as a main source and the converters are controlled with a single real time dSPACE board as an interface between control part and electrical part. It is worth to note that the physical parameters are chosen based on the [21] in order to have an accurate comparison and verified the experimental results.

The setup for the experimental tests is depicted in Fig. 12, which consists of two VSCs, LC filters $C_f = 15\ \mu F$, $L_f = 2.4\ mH$ and nominal voltage $V_{nom} = 200\ V$, $f_{nom} = 50\ Hz$.

The performance of the proposed distributed control structure in active and reactive power sharing during the load change are illustrated in Fig. 13. Like the simulations, at $t = 60\ ms$ a load is added to the MG setup and consequently, two VSCs follow the load change immediately. This figure depicts that active and reactive power can be shared accurately between two VSCs. Thus, by employing FCS-MPC and only local controllers, fast and accurate power sharing between two VSCs have been carried out.

This article has been accepted for publication in a future issue of this journal, but has not been fully edited. Content may change prior to final publication. Citation information: DOI 10.1109/TPEL.2019.2896955, IEEE Transactions on Power Electronics

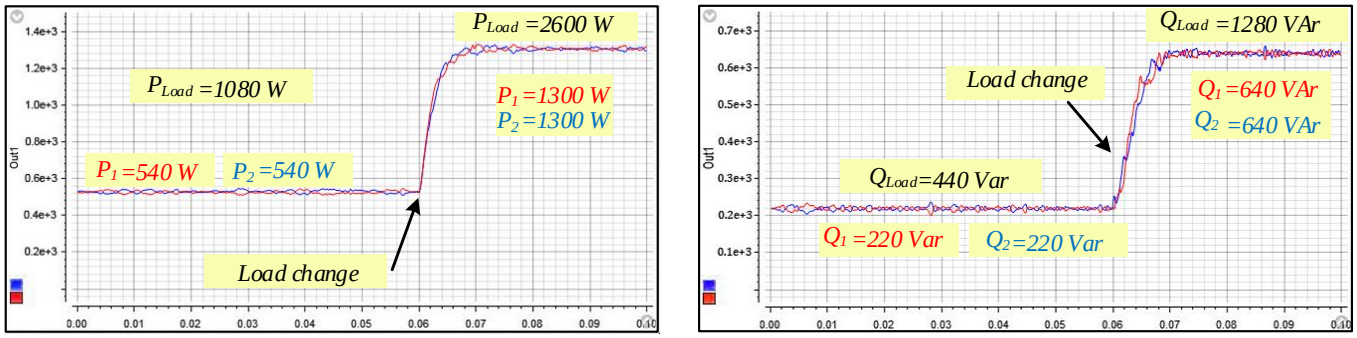

(a) Active power sharing (b) Reactive power sharing

Fig. 13. Experimental validation of the proposed control structure of an islanded microgrid with two VSCs. (a) Active power sharing accuracy. (b) Reactive power sharing accuracy during a load change.

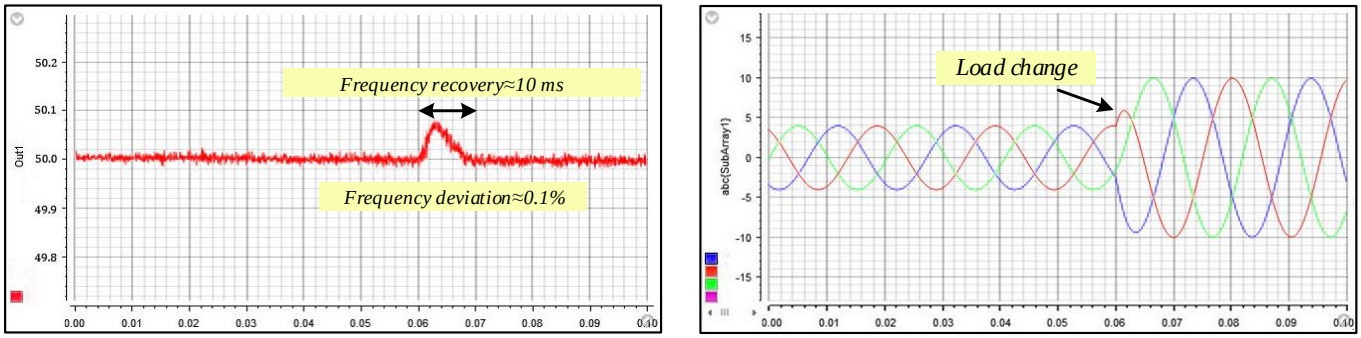

(a) (b)

Fig. 14. Evaluation of the proposed distributed SC structure. (a) Frequency recovery during a load step. (b) Measured current at the point of common coupling from the dSPACE control desk.

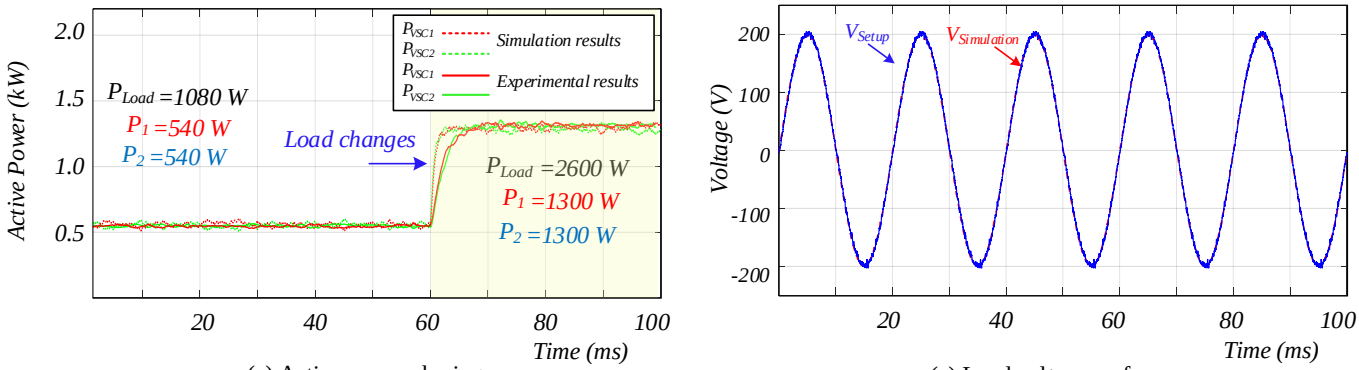

(a) Active power sharing (a) Load voltage performance

Fig. 15. Comprehensive comparison between experimental and simulation results. (a) Active power sharing (b) voltage restoration.

In order to evaluate the effectiveness of the proposed approach to compensate for frequency deviations a step load is added to the MG setup to changes the frequency. Fig. 14(a) shows the frequency deviation and the fast restoration process. As it can be seen, after the step load change, the MG reaches steady state almost immediately and frequency deviation is recovered during a period of 10 ms.

Fig. 14 (b) shows the current waveform at the point of common coupling (load side). As seen at t=60 ms, the current waveform accurately follows the load change. Consequently, the experimental results also validate the fast dynamic performance of the proposed distributed control structure. In Fig. 15 (a) a comparison between the simulated power sharing and experimental results is shown. Due to the required processing time to execute the code, in the practical implementation approximately 3 ms slower response can be seen, which is neglectable compared to the conventional approaches. Furthermore, a comparison between the simulation result and experiments for load voltage regulation is shown in Fig. 15 (b). As it can be seen, both experimental and simulation results verified accurate voltage regulation.

VI. Conclusion

In this paper, a distributed secondary control structure for power electronic based ac MG has been proposed. Firstly, a FCS-MPC strategy is applied in inner primary control level in order to regulate the voltage of power converters. By utilizing FCS-MPC for paralleled VSCs the voltage regulation of converters is improved with fast transient response. Hence, the upper control level can be performed with a high bandwidth. Then, a distributed secondary control is applied based on the local averaging, while a wireless communication in upper stage shares the required data among VSCs. The FCS-MPC based control strategy combined with distributed operation not only makes the MG very robust, but improves also the dynamic performance. The concept has been evaluated experimentally on a dual VSCs setup. Indeed, the results confirms that the proposed control structure compensates for voltage and frequency deviations with far superior dynamic performance compared to the state of the art using linear control structures.

References

[1] S. Parhizi, H. Lotfi, A. Khodaei, and S. Bahramirad, "State of the art in research on microgrids: A review," *IEEE Access*, vol. 3, pp. 890–925, 2015.

[2] R. H. Lasseter, "Smart distribution: Coupled microgrids," *Proceedings of the IEEE*, vol. 99, no. 6, pp. 1074–1082, 2011.

[3] A. Khodaei, "Microgrid optimal scheduling with multi-period islanding constraints," *IEEE Trans. Power Syst.*, vol. 29, no. 3, pp. 1383–1392, 2014.

[4] W. Su, J. Wang, and J. Roh, "Stochastic energy scheduling in microgrids with intermittent renewable energy resources," *IEEE Trans. Smart Grid*, vol. 5, no. 4, pp. 1876–1883, 2014.

[5] M. Marzband, E. Yousefnejad, A. Sumper, and J. L. Domínguez-García, "Real time experimental implementation of optimum energy management system in standalone microgrid by using multi-layer ant colony optimization," *International Journal of Electrical Power & Energy Systems*, vol. 75, pp. 265–274, 2016.

[6] A. Khodaei, S. Bahramirad, and M. Shahidehpour, "Microgrid planning under uncertainty," *IEEE Trans. Power Syst.*, vol. 30, no. 5, pp. 2417–2425, 2015.

[7] Y. Guo, J. Xiong, S. Xu, and W. Su, "Two-stage economic operation of microgrid-like electric vehicle parking deck," *IEEE Trans. Smart Grid*, vol. 7, no. 3, pp. 1703–1712, 2016.

[8] D. E. Olivares, A. Mehrizi-Sani, A. H. Etemadi, C. A. Cañizares, R. Iravani, M. Kazerani, A. H. Hajimiragha, O. Gomis-Bellmunt, M. Saeedifard, R. Palma-Behnke, *et al.*, "Trends in microgrid control," *IEEE Trans. Smart Grid*, vol. 5, no. 4, pp. 1905–1919, 2014.

[9] J. M. Guerrero, J. C. Vasquez, J. Matas, L. G. De Vicuña, and M. Castilla, "Hierarchical control of droop-controlled ac and dc microgridsa general approach toward standardization," *IEEE Trans. Ind. Electron*, vol. 58, no. 1, pp. 158–172, 2011.

[10] J. P. Lopes, C. Moreira, and A. Madureira, "Defining control strategies for microgrids islanded operation," *IEEE Trans. Power Syst.*, vol. 21, no. 2, pp. 916–924, 2006.

[11] Y. A.-R. I. Mohamed and A. A. Radwan, "Hierarchical control system for robust microgrid operation and seamless mode transfer in active distribution systems," *IEEE Trans. Smart Grid*, vol. 2, no. 2, pp. 352–362, 2011.

[12] J. Kim, J. M. Guerrero, P. Rodriguez, R. Teodorescu, and K. Nam, "Mode adaptive droop control with virtual output impedances for an inverter-based flexible ac microgrid," *IEEE Trans. Power Electron.*, vol. 26, no. 3, pp. 689–701, 2011.

[13] S. Anand, B. G. Fernandes, and J. Guerrero, "Distributed control to ensure proportional load sharing and improve voltage regulation in low-voltage dc microgrids," *IEEE Trans. Power Electron.*, vol. 28, no. 4, pp. 1900–1913, 2013.

[14] J. Schiffer, T. Seel, J. Raisch, and T. Sezi, "Voltage stability and reactive power sharing in inverter-based microgrids with consensus-based distributed voltage control," *IEEE Trans. Control Syst. Technol.*, vol. 24, no. 1, pp. 96–109, 2016.

[15] J. C. Vasquez, J. M. Guerrero, M. Savaghebi, J. Eloy-Garcia, and R. Teodorescu, "Modeling, analysis, and design of stationary-reference-frame droop-controlled parallel three-phase voltage source inverters," *IEEE Trans. Ind. Electron*, vol. 60, no. 4, pp. 1271–1280, 2013.

[16] A. Micallef, M. Apap, C. Spiteri-Staines, J. M. Guerrero, and J. C. Vasquez, "Reactive power sharing and voltage harmonic distortion compensation of droop controlled single phase islanded microgrids," *IEEE Trans. Smart Grid*, vol. 5, no. 3, pp. 1149–1158, 2014.

[17] N. M. Dehkordi, N. Sadati, and M. Hamzeh, "Distributed robust finite-time secondary voltage and frequency control of islanded microgrids," *IEEE Trans. Power Syst.*, vol. 32, no. 5, pp. 3648–3659, 2017.

[18] J. M. Guerrero, M. Chandorkar, T.-L. Lee, and P. C. Loh, "Advanced control architectures for intelligent microgridspart i: Decentralized and hierarchical control," *IEEE Trans. Ind. Electron*, vol. 60, no. 4, pp. 1254–1262, 2013.

[19] M. Savaghebi, A. Jalilian, J. C. Vasquez, and J. M. Guerrero, "Secondary control scheme for voltage unbalance compensation in an islanded droop-controlled microgrid," *IEEE Trans. Smart Grid*, vol. 3, no. 2, pp. 797–807, 2012.

[20] S. Peyghami, H. Mokhtari, P. C. Loh, P. Davari, and F. Blaabjerg, "Distributed primary and secondary power sharing in a droop-controlled lvdc microgrid with merged ac and dc characteristics," *IEEE Trans. Smart Grid*, 2016.

[21] Q. Shafiee, J. M. Guerrero, and J. C. Vasquez, "Distributed secondary control for islanded microgridsa novel approach," *IEEE Trans. Power Electron.*, vol. 29, no. 2, pp. 1018–1031, 2014.

[22] C. Yuen, A. Oudalov, and A. Timbus, "The provision of frequency control reserves from multiple microgrids," *IEEE Trans. Ind. Electron*, vol. 58, no. 1, pp. 173–183, 2011.

[23] A. Bidram, A. Davoudi, F. L. Lewis, and J. M. Guerrero, "Distributed cooperative secondary control of microgrids using feedback linearization," *IEEE Trans. Power Syst.*, vol. 28, no. 3, pp. 3462–3470, 2013.

[24] F. Guo, C. Wen, J. Mao, and Y.-D. Song, "Distributed secondary voltage and frequency restoration control of droop-controlled inverter-based microgrids," *IEEE Trans. Ind. Electron*, vol. 62, no. 7, pp. 4355–4364, 2015.

[25] J. W. Simpson-Porco, Q. Shafiee, F. Dörfler, J. C. Vasquez, J. M. Guerrero, and F. Bullo, "Secondary frequency and voltage control of islanded microgrids via distributed averaging," *IEEE Trans. Ind. Electron*, vol. 62, no. 11, pp. 7025–7038, 2015.

[26] T. Dragičević, "Model predictive control of power converters for robust and fast operation of ac microgrids," *IEEE Trans. Power Electron.*, vol. 33, no. 7, pp. 6304–6317, 2018.

[27] T. Dragicevic, R. Heydari, and F. Blaabjerg, "Super-high bandwidth secondary control of ac microgrids," in *Applied Power Electronics Conference and Exposition (APEC)*, IEEE, 2018.

[28] J. Rocabert, A. Luna, F. Blaabjerg, and P. Rodriguez, "Control of power converters in ac microgrids," *IEEE Trans. Power Electron.*, vol. 27, no. 11, pp. 4734–4749, 2012.

[29] R. Firestone and C. Marnay, "Energy manager design for microgrids," *Lawrence Berkeley National Laboratory*, 2005.

[30] A. Mehrizi-Sani and R. Iravani, "Potential-function based control of a microgrid in islanded and grid-connected modes," *IEEE Trans. Power Syst.*, vol. 25, no. 4, pp. 1883–1891, 2010.

[31] H. Karimi, H. Nikkhajoei, and R. Iravani, "Control of an electronically-coupled distributed resource unit subsequent to an islanding event," *IEEE Trans. Power Del.*, vol. 23, no. 1, pp. 493–501, 2008.

[32] H. Nikkhajoei and R. H. Lasseter, "Distributed generation interface to the certs microgrid," *IEEE Trans. Power Del.*, vol. 24, no. 3, pp. 1598–1608, 2009.

[33] A. Bidram and A. Davoudi, "Hierarchical structure of microgrids control system," *IEEE Trans. Smart Grid*, vol. 3, no. 4, pp. 1963–1976, 2012.

[34] G. Escobar, P. Mattavelli, A. M. Stankovic, A. A. Valdez, and J. Leyva-Ramos, "An adaptive control for ups to compensate unbalance and harmonic distortion using a combined capacitor/load current sensing," *IEEE Trans. Ind. Electron*, vol. 54, no. 2, pp. 839–847, 2007.

[35] A. Hasanzadeh, O. C. Onar, H. Mokhtari, and A. Khaligh, "A proportional-resonant controller-based wireless control strategy with a reduced number of sensors for parallel-operated upss," *IEEE Trans. Power Del.*, vol. 25, no. 1, pp. 468–478, 2010.

[36] R. Heydari, M. Alhasheem, T. Dragicevic, and F. Blaabjerg, "Model predictive control approach for distributed hierarchical control of vsc-based microgrids," in *20th European Conference on Power Electronics and Applications (EPE'18 ECCE Europe)*, IEEE, 2018.

[37] Q.-C. Zhong, "Robust droop controller for accurate proportional load sharing among inverters operated in parallel," *IEEE Trans. Ind. Electron*, vol. 60, no. 4, pp. 1281–1290, 2013.

[38] E. Rokrok and M. Golshan, "Adaptive voltage droop scheme for voltage source converters in an islanded multibus microgrid," *IET generation, transmission & distribution*, vol. 4, no. 5, pp. 562–578, 2010.
[39] G. Diaz, C. Gonzalez-Moran, J. Gomez-Aleixandre, and A. Diez, "Scheduling of droop coefficients for frequency and voltage regulation in isolated microgrids," *IEEE Trans. Power Syst.*, vol. 25, no. 1, pp. 489–496, 2010.
[40] B. Awad, J. Wu, and N. Jenkins, "Control of distributed generation," *e & i Elektrotechnik und Informationstechnik*, vol. 125, no. 12, pp. 409–414, 2008.
[41] T. Dragicevic and M. Novak, "Weighting factor design in model predictive control of power electronic converters: An artificial neural network approach," *IEEE Trans. Ind. Electron*, 2018.
[42] Q. Shafiee, C. Stefanovic, T. Dragicevic, P. Popovski, J. C. Vasquez, and J. M. Guerrero, "Robust networked control scheme for distributed secondary control of islanded microgrids," *IEEE Trans. Ind. Electron*, vol. 61, no. 10, pp. 5363–5374, 2014.
[43] F. De Bosio, L. A. de Souza Ribeiro, F. D. Freijedo, M. Pastorelli, and J. M. Guerrero, "Effect of state feedback coupling and system delays on the transient performance of stand-alone vsi with lc output filter," *IEEE Trans. Ind. Electron*, vol. 63, no. 8, pp. 4909–4918, 2016.
[44] T. Dragicevic, "Dynamic stabilization of dc microgrids with predictive control of point of load converters," *IEEE Trans. Power Electron*, 2018.
[45] J.-J. E. Slotine, W. Li, *et al.*, *Applied nonlinear control*, vol. 199. Prentice hall Englewood Cliffs, NJ, 1991.

Rasool Heydari (S'16) received the B.Sc. degree in electrical engineering, and the M.Sc. degree in power system engineering in 2011 and 2014, respectively. He is currently working toward the Ph.D. degree in advanced control of the power electronic based power systems and microgrids at the Department of Energy Technology, Aalborg University, Denmark. He is also a visiting researcher with ABB Corporate Research, Västerås, Sweden. His principal field of interest is control, stability and dynamic analysis of power electronic systems, mainly distributed and grid-connected converters and microgrid.

Tomislav Dragicevic (S'09-M'13-SM'17) received the M.Sc. and the industrial Ph.D. degrees in Electrical Engineering from the Faculty of Electrical Engineering, Zagreb, Croatia, in 2009 and 2013, respectively. From 2013 until 2016 he has been a Postdoctoral research associate at Aalborg University, Denmark. From March 2016 he is an Associate Professor at Aalborg University, Denmark where he leads an Advanced Control Lab. He made a guest professor stay at Nottingham University, UK during spring/summer of 2018. His principal field of interest is design and control of microgrids, and application of advanced modeling and control concepts to power electronic systems. He has authored and co-authored more than 155 technical papers (more than 55 of them are published in international journals, mostly IEEE Transactions) in his domain of interest, 8 book chapters and a book in the field. He serves as Associate Editor in the IEEE TRANSACTIONS ON INDUSTRIAL ELECTRONICS, in IEEE Emerging and Selected Topics in Power Electronics and in the Journal of Power Electronics. Dr. Dragievi is a recipient of the Konar prize for the best industrial PhD thesis in Croatia, and a Robert Mayer Energy Conservation award.

Frede Blaabjerg (S'86M'88SM'97F'03) was with ABB-Scandia, Randers, Denmark, from 1987 to 1988. From 1988 to 1992, he got the PhD degree in Electrical Engineering at Aalborg University in 1995. He became an Assistant Professor in 1992, an Associate Professor in 1996, and a Full Professor of power electronics and drives in 1998. From 2017 he became a Villum Investigator. He is honoris causa at University Politehnica Timisoara (UPT), Romania and Tallinn Technical University (TTU) in Estonia.

His current research interests include power electronics and its applications such as in wind turbines, PV systems, reliability, harmonics and adjustable speed drives. He has published more than 600 journal papers in the fields of power electronics and its applications. He is the co-author of four monographs and editor of ten books in power electronics and its applications.

He has received 30 IEEE Prize Paper Awards, the IEEE PELS Distinguished Service Award in 2009, the EPE-PEMC Council Award in 2010, the IEEE William E. Newell Power Electronics Award 2014 and the Villum Kann Rasmussen Research Award 2014. He was the Editor-in-Chief of the IEEE TRANSACTIONS ON POWER ELECTRONICS from 2006 to 2012. He has been Distinguished Lecturer for the IEEE Power Electronics Society from 2005 to 2007 and for the IEEE Industry Applications Society from 2010 to 2011 as well as 2017 to 2018. In 2019-2020 he serves a President of IEEE Power Electronics Society. He is Vice-President of the Danish Academy of Technical Sciences too. He is nominated in 2014-2018 by Thomson Reuters to be between the most 250 cited researchers in Engineering in the world.